

ARTICLE

Received 27 Nov 2013 | Accepted 4 Mar 2014 | Published 27 Mar 2014

DOI: 10.1038/ncomms4548

Tunable plasmons in atomically thin gold nanodisks

A. Manjavacas^{1,†} & F.J. García de Abajo^{2,3}

The ability to modulate light at high speeds is of paramount importance for telecommunications, information processing and medical imaging technologies. This has stimulated intense efforts to master optoelectronic switching at visible and near-infrared frequencies, although coping with current computer speeds in integrated architectures still remains a major challenge. As a partial success, mid-infrared light modulation has been recently achieved through gating patterned graphene. Here we show that atomically thin noble metal nanoislands can extend optical modulation to the visible and near-infrared spectral range. We find plasmons in thin metal nanodisks to produce similar absorption cross-sections as spherical particles of the same diameter. Using realistic levels of electrical doping, plasmons are shifted by about half their width, thus leading to a factor-of-two change in light absorption. These results, which we substantiate on microscopic quantum theory of the optical response, hold great potential for the development of electrical visible and near-infrared light modulation in integrable, nanoscale devices.

¹IQFR—CSIC, Serrano 119, 28006 Madrid, Spain. ²ICFO—Institut de Ciències Fotòniques, Mediterranean Technology Park, 08860 Castelldefels (Barcelona), Spain. ³ICREA—Institut Català de Recerca i Estudis Avançats, Passeig de Lluís Companys 23, 08010 Barcelona, Spain. † Present address: Department of Physics and Astronomy and Laboratory for Nanophotonics, Rice University, Houston, Texas 77005, USA. Correspondence and requests for materials should be addressed to F.J.G.d.A. (email: javier.garciadeabajo@icfo.es).

Surface plasmons, the collective oscillations of conduction electrons in metallic structures, allow us to confine light down to deep subwavelength volumes¹. In addition, they couple strongly to electromagnetic fields². Because of these properties, plasmons are excellent tools to engineer nanoscale devices for manipulating optical signals, without the limitation imposed by diffraction in far-field set-ups. This has triggered a number of applications in areas as diverse as ultrasensitive biosensing³, improved photovoltaics⁴, plasmon-enhanced photodetection⁵ and photothermal cancer therapy⁶. The design of plasmonic structures with suitable spectral characteristics involves a careful choice of geometry and composition. In recent years, a vast amount of work has been devoted to producing nanostructures made of noble metals with controlled size and morphology, using in particular colloidal methods⁷ and lithography⁸.

Despite these advances in the control over the static characteristics of plasmons, the dynamical modulation of their frequencies and spatial profiles remains elusive, particularly in the visible and near-infrared (vis-NIR) parts of the spectrum. In this context, slow mild changes of the plasmon frequency have been produced by electrochemically injecting electrons in metal nanoparticles⁹, by electrically driving liquid crystals containing plasmonic particles¹⁰, and through controllable metamaterial designs^{11,12}. Magneto-optical modulation has also been explored to control plasmons in noble metal structures¹³. Hybrids of plasmonic and conductive oxides have been proposed^{14,15}, as well as colloids based on different materials¹⁶. However, we still need to devise new methods to produce larger and faster control over plasmons, as required for nanoscale optical commutation and light modulation at high speeds.

Recently, the emergence of graphene¹⁷ as a novel plasmonic material^{18–20} has opened up new paths towards the design of dynamically tunable plasmonic devices. Electrically doped graphene supports surface plasmons whose frequency can be efficiently varied by changing the level of doping^{21–23}. Consequently, the resulting modulation is intrinsically fast because it can be driven by charge-carrier injection using conventional electric gating technology. This promising material has been so far shown to support mid-infrared and lower-frequency plasmons^{21–25}, while vis-NIR modes are being pursued by reducing the size of the structures^{26,27} and increasing the level

of doping²³. The search for plasmon modulation in the vis-NIR is thus still ongoing, as these are spectral regions of utmost importance for sensing and optical signal processing technologies.

The origins of the excellent tunability of plasmons in graphene can be found in both the atomic thickness and the peculiar electronic structure of this material. The latter is characterized by a linear dispersion relation, which leads to a vanishing of the density of states at the Fermi level, so that a relatively small density of injected charge carriers produces substantial optical gaps in which collective plasmon modes emerge^{17,19}. Although this unique feature cannot be easily transported to conventional plasmonic materials, such as gold, we can still mimic graphene plasmonics by going to atomically thin noble metals, whose optical response should be more susceptible to doping than traditional thicker layers. In particular, monolayer gold, the synthesis of which has been mastered for a long time in the context of surface science²⁸, presents the advantage of having a plasma frequency compatible with the existence of plasmons in the vis-NIR²⁹.

Here we show that single-monolayer gold disks (SMGDs) with diameters of the order of 10 nm support surface plasmons with large cross-sections comparable to their geometrical areas. The frequencies of these excitations lie in the vis-NIR and can be efficiently modulated using attainable concentrations of doping charge carriers, which can be provided via electrical doping using, for example, backgating technology. We also analyse the optical response of periodic arrays of SMGDs, for which we predict an absorbance $\sim 25\%$ for metal layer filling fractions $\sim 40\%$.

Results

Electrically tunable optical response. The system under study is depicted in Fig. 1a. We consider a gold nanodisk of diameter D , extracted from a single (111) atomic layer of gold. We take the thickness of the gold monolayer to be equal to the separation between (111) atomic planes in bulk gold (that is, $a_0/\sqrt{3}$, where $a_0 = 0.408$ nm is the atomic lattice constant). Incidentally, our results are rather independent of the choice of disk thickness when this is small compared with the diameter, as long as the total valence charge is preserved (see Supplementary Fig. 1). As a first step in our analysis, we simulate the optical response of a SMGD classically by modelling it as a thin disk described by

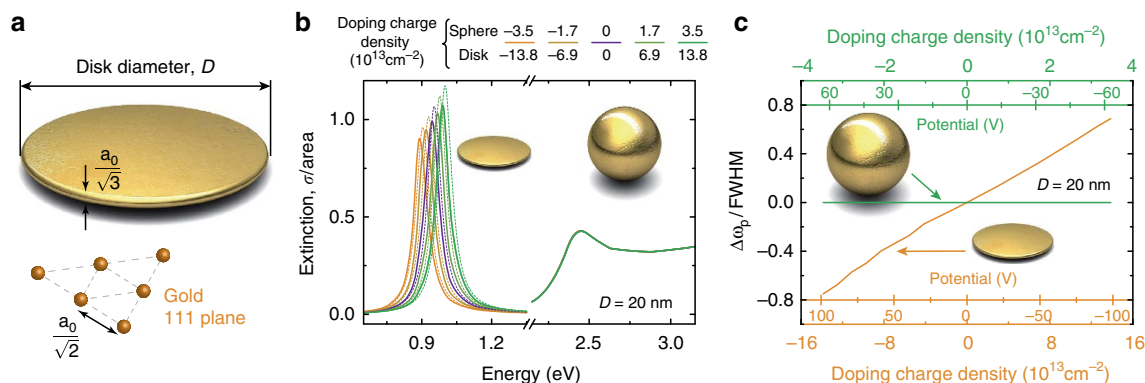


Figure 1 | Optical response and electrical tunability of SMGDs. (a) We consider a SMGD of diameter D carved from a single (111) atomic layer. The disk thickness is $a_0/\sqrt{3}$, where $a_0 = 0.408$ nm is the atomic lattice constant. (b) Extinction cross-section of a $D=20$ nm SMGD for different doping charge-carrier densities (see upper legend). A doping density of 13.8×10^{13} cm⁻² corresponds to a total of 443 additional charge carriers in the disk. For comparison, we also plot the cross-section for a gold nanosphere of the same diameter and total doping charge, clearly showing an almost negligible degree of tunability. The particles are assumed to be homogeneously doped and described classically through the local dielectric function tabulated from measured optical data (solid curves)²⁹. Results obtained from a Drude dielectric function (equation (1)) are shown for comparison (broken curves). (c) Plasmon frequency shift relative to the width of the plasmon resonance for the disk (orange) and the sphere (green) of panel b as a function of doping density. The small scales indicate the potential at the disk/sphere surface for different disk doping densities.

a frequency-dependent homogenous dielectric function $\epsilon(\omega)$. More precisely, we calculate the extinction cross-section σ by solving Maxwell's equations using the boundary-element method³⁰. Interestingly, for a diameter $D=20$ nm, the cross-section is dominated by a NIR plasmon at an energy ~ 1 eV and it exceeds the geometrical area of the disk (see left part of Fig. 1b).

It is convenient to separate the contribution from s -band electrons in the dielectric function as a Drude term,

$$\epsilon(\omega) = \epsilon_b - \frac{\omega_p^2}{\omega(\omega + i\gamma)}, \quad (1)$$

where ϵ_b accounts for the effect of background screening due to d -band electrons, $\hbar\omega_p = 9.06$ eV is the classical plasmon energy associated with s -valence electrons (see Methods), and $\hbar\gamma = 71$ meV is an inelastic width (we adopt this value of the damping throughout this work). As explained below, we introduce doping in the classical model by changing ω_p in equation (1). In general, the description of the response of gold in the vis-NIR region including interband transitions requires to use either experimental data²⁹ or a sophisticated multi-Lorentzian model³¹ for $\epsilon(\omega)$, which yields a ω -dependent background $\epsilon_b = \epsilon(\omega) + \omega_p^2/[\omega(\omega + i\gamma)]$. However, we show in Fig. 1b that a simple Drude model for equation (1) (dashed curves), consisting in fixing $\epsilon_b = 9.5$ for all frequencies, produces a satisfactory level of accuracy at the observed relatively low disk-plasmon energies compared with the results obtained from tabulated optical data²⁹ (solid curves). In addition, as the Drude model (that is, constant ϵ_b) provides a natural connection with the quantum mechanical approach described below, we use it for disks in what follows.

We consider next the effect of electrical doping. The spatial distribution of additional charge carriers depends on the doping configuration, as it can be, for example, homogenous for disks connected to a non-absorbing gate (for example, indium tin oxide) or inhomogenous in self-standing charged disks, although the plasmon energies and spatial profiles are expected to be similar in both cases based on our experience with graphene disk plasmons³². For simplicity, we assume homogeneously doped disks in what follows. The additional doping charge density n adds up to the undoped s -band density $n_0 = m_e\omega_p^2/(4\pi e^2)$, which yields an areal electron density $n_0a_0/\sqrt{3} \approx 1.4 \times 10^{15} \text{ cm}^{-2}$ that is rather close to the s -band areal electron density in neutral monolayer gold, $4/\sqrt{3}a_0^2$. The doping charge is thus introduced by changing the bulk plasma frequency to $\omega_p = [(4\pi e^2/m_e)(n_0 + n)]^{1/2}$ in equation (1). Now, the addition of a moderate amount of doping electrons (~ 5 – 10% of n_0) results in significant blue shifts and increase in the strength of the plasmon resonance (*cf.* purple and green curves of Fig. 1b). Obviously, the injection of similar amounts of holes produces the opposite effects (Fig. 1b, orange curve). The small thickness of the disk is a key factor in producing such dramatic modifications in the optical response using realistic doping densities. In fact, repeating this operation with a gold nanosphere of the same diameter, we also observe a prominent plasmon (Fig. 1b, ~ 2.5 eV region), but it remains unchanged when adding similar amounts of doping charges. In the sphere, the doping charges pile up in the outermost atomic layer³³, but this produces the same extinction cross-section as if the charges were homogeneously distributed over its entire volume and, therefore, the change in bulk charge density is substantially reduced with respect to the disk.

Figure 1c compares the modulation of the nanodisk and the sphere. In particular, we plot the frequency shift normalized to the full width at half maximum (FWHM) for the plasmon resonance as a function of doping charge density. In contrast to the negligible tunability of the sphere, the disk allows shifts comparable to the FWHM to be electrically induced. Incidentally,

the doping densities here considered produce realistic values of the electrostatic potential at the surface of these nanoparticles (Fig. 1c, small scales), indicating that they are compatible with currently available gating technology²³.

Quantum mechanical effects. For nanoparticles of only a few nanometres in size, the above classical description fails to account for spatial dispersion and quantum confinement effects^{34,35}, which generally require models based on a quantum mechanical treatment of valence electrons and their interactions. Here we use the random-phase approximation (RPA) to calculate the optical response of SMGDs (see Methods) within the electrostatic approximation, which should be rather accurate, given the small sizes of the particles under consideration. This allows us to determine the validity of the classical approach and explore the response of nanodisks with smaller diameters.

We use particle-in-a-box states to describe independent s -band electrons. The cylindrical box has the same dimensions as in the classical calculations (see above) and it is surrounded by an infinite potential. The RPA susceptibility is then evaluated using these electron states to obtain the induced charge density, which in turn allows us to compute the optical extinction of the disk. In addition, we model screening due to d -band electrons through an array of point dipoles placed at the atomic positions in the (111) layer and with polarizability adjusted to render an effective background permittivity ϵ_b in the bulk material (see Methods). Apart from the relative position of these dipoles with respect to the disk centre, our quantum description only depends on the three same parameters as the classical Drude theory (that is, ϵ_b , ω_p and γ).

A major assumption we are making is that γ takes the same value as in the bulk metal. We use this as a reasonable estimate because s -band electrons are rather delocalized along directions parallel to the layer (that is, similar to the bulk), while they are narrowly confined to the ground state across the transversal direction, so that plasmons result from in-plane motion. However, the actual value of γ might depend on the detailed coupling of valence electrons to impurities and to the atomic lattice. Concerning d -band screening, our effective-dipoles approach should provide a more realistic description than a homogenous polarizable background. Although the discreteness of the dipole lattice can have strong effects in small islands, we find converged results for large islands, which are independent of the alignment of the dipole lattice relative to the disk centre.

Figure 2 shows the extinction cross-section normalized to the disk area for SMGDs of different diameters ranging from 3 to 15 nm. The main conclusions from this figure are as follows: (1) the extinction cross-sections are of the order of the disk area; (2) the plasmon energy increases with decreasing diameter D , exhibiting an approximate $\propto 1/\sqrt{D}$ dependence, similar to what one finds in graphene nanodisks²³; (3) quantum calculations produce energies above those predicted by classical theory, as well as broader plasmon peaks, but the discrepancy between the two models decreases with increasing diameter; (4) in the absence of d -band screening (Fig. 2a, obtained by setting $\epsilon_b = 1$), both levels of description give rise to smooth plasmon peaks, in contrast to the quantum results obtained when d -band screening is switched on (Fig. 2b, with $\epsilon_b = 9.5$); (5) d -band screening also leads to a redshift of the plasmons, which is more pronounced at small sizes. Incidentally, the induced charge associated with the plasmon exhibits a dipolar profile dressed with radial oscillations mimicking those of Friedel oscillations, which are particularly intense for small diameters (see Supplementary Fig. 2).

Similar blue shifts with respect to classical local theory are also found in small noble metal particles³⁶, the origin of which is a

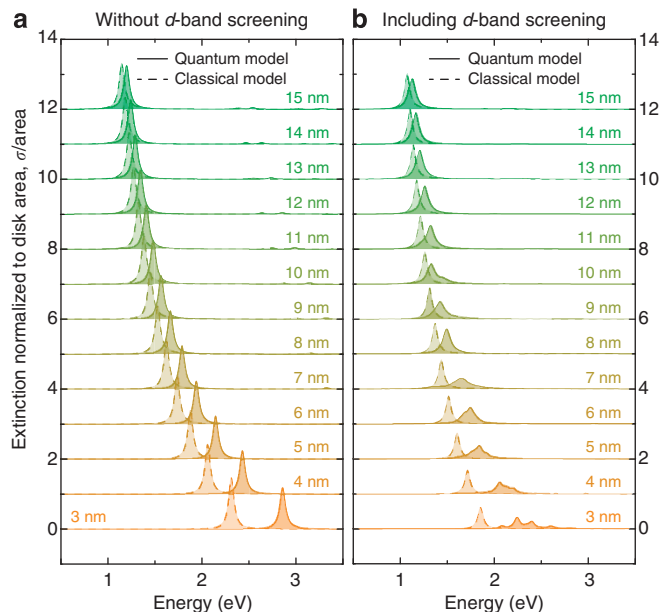


Figure 2 | Optical response of individual SMGDs. We plot the extinction cross-section normalized to the geometrical area for different diameters D , calculated using the quantum model (solid curves) and a classical description (dashed curves). Results obtained with and without inclusion of d -band screening are shown in **b** and **a**, respectively.

combination of non-local and quantum effects, particularly owing to the surface spill out of s electrons beyond the polarizable background of d -band electrons. In simple metals such as aluminium, the spill out produces smaller electron densities near the surface and, consequently, also smaller surface plasmon frequencies. In contrast, in noble metals, the spill out results in a weaker interaction with the localized d electrons and, thus, it leads to an increase in the observed frequency, which overcomes the redshift due to the smaller electron density³⁷. We incorporate here the finite extension of s electrons across the normal direction, combined with the localization of the effective d -band dipoles, leading to similar blue shifts. Interestingly, our quantum model predicts splitting of the plasmon into multiple peaks for small disks when d -band screening is included (see for example, the $D = 3$ nm spectrum in Fig. 2b). The presence of these peaks, which are rapidly coalescing into a single plasmon resonance for $D > 8$ nm, is a manifestation of the discrete character of the interaction with d -band electrons, which is more pronounced for small D 's. The jumps observed in the FWHM also shares a similar origin. It should be noted that these effects could be sensitive to the exact form of the s -electron transversal wave function in the smallest islands under consideration, which require a more atomistic analysis, based, for example, on density functional theory^{38–40}. Similarly, the spectra for the smallest disks depend on the alignment of the d -band dipole lattice relative to the edges. In practice, one-dimensional faceting of the edges becomes an important source of anisotropy, which can contribute to broaden the spectra for $D < 5$ nm.

The convergence of the quantum model to the classical description for increasing diameter is clearly observed in Fig. 3, which summarizes the plasmon energies and widths observed in the spectra of Fig. 2. Here we define the FWHM as the frequency interval around the peak maximum that contains half of its area; this definition coincides with the standard FWHM for individual Lorentzian resonances, but it can be applied to multiple resonances as well to yield an overall width (in particular to the lower quantum-model spectra of Fig. 2b). Within the electrostatic

limit under consideration, the FWHM predicted by the classical model is independent of diameter and equals the damping energy $\hbar\gamma = 71$ meV (see equation (1)). In contrast, the quantum model leads to a significant increase in the FWHM for small diameters, essentially as a consequence of Landau damping, which involves inelastic decay of plasmons to electron-hole pairs for momentum transfers $\sim \omega/v_F$, where v_F is the Fermi velocity ($\sim 10^6$ m s⁻¹, see Supplementary Fig. 3a). As the momentum transfer provided by the breaking of translational invariance in a disk is $\sim 2\pi/D$, the onset of Landau damping is expected to occur at $D \sim 2\pi v_F/\omega \sim 4$ nm, in qualitative agreement with the results shown in Fig. 3c,d. An intuitive estimate can be established from the electron mean free path $v_F/\gamma \sim 10$ nm, which determines the rate of collisions with the edges (that is, events that provide the noted momentum), and is also in agreement with the trends observed in Fig. 3c,d, although the value of γ regarded as a parameter simply produces an additional contribution to the FWHM that is independent of D , and the ultimate origin of broadening for small sizes can be found in Landau damping.

As discussed in Fig. 1, the optical response of SMGDs can be modified through the addition of small amounts of charge carriers to relatively large disks ($D = 20$ nm), for which classical theory is rather accurate (see Figs 2 and 3). Using smaller SMGDs, we obtain qualitatively similar results as for larger disks (see Fig. 4 for an analysis of a $D = 8$ nm doped disk). Given the small disk size, we compare classical (Fig. 4d–f) and quantum (Fig. 4a–c) results, showing again a blue shift and plasmon broadening in the latter relative to the former.

In contrast to the nearly linear plasmon shift with doping charge density predicted by classical theory (Fig. 4e), the quantum model leads to initially smaller modulation at low doping (Fig. 4b), which increases to a faster pace than the classical results for higher doping. This nonlinear dependence of the plasmon energy on the doping density could be exploited for improved light modulation by operating around a highly doped SMGD configuration. In particular, the plasmon shift can be as large as the FWHM when the density of s -band electrons is changed by $\pm(5\text{--}10)\%$.

Interestingly, the nonlinear plasmon shifts observed in the quantum model become oscillatory when examining the maximum extinction cross-section and the FWHM (Fig. 4c). The oscillations of these two quantities are out of phase, as required to satisfy the f -sum rule⁴¹, and can be traced back to the discreteness of the electronic energies. Importantly, in all cases the maximum cross-section is of the order of the disk area (Fig. 4c,f), thus providing good coupling to light for potential applications to modulation devices.

Periodic arrangement of single-monolayer gold nanodisks. The large optical strength and degree of electrical tunability discussed above for SMGDs can be exploited to modulate light that is either transmitted or reflected by a periodic array of such structures. We consider a hexagonal array of $D = 8$ nm disks in Fig. 5 with different values of the array spacing d . Given the large mismatch between D and the resonant light wavelength (~ 830 nm), we approximate the disks as point dipoles of polarizability extracted as explained in Methods (see also Supplementary Fig. 4, where we show that higher-order multipoles play only a small role for the relative distances under consideration). Following previous analytical methods⁴² to compute the absorbance A , we find remarkably large values (for example, $A = 25\%$ for $d = 1.5D$, see Fig. 5b), given the small amount of gold in the structure (sub-monoatomic layer film). The fractional change in absorbance driven by electrical doping (Fig. 5c) is rather independent of lattice spacing and reaches $\sim 70\%$ for a 10% variation in the

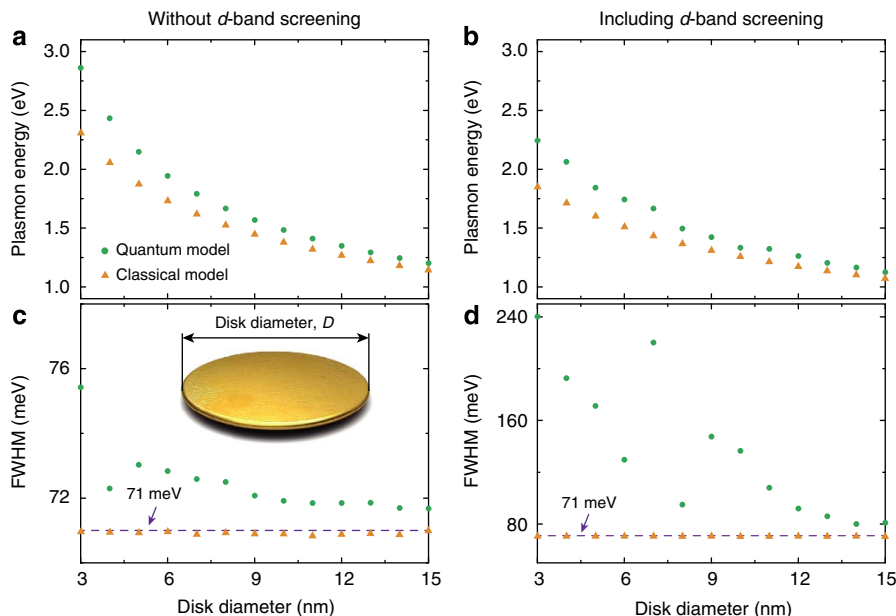


Figure 3 | Comparison of quantum and classical plasmon energies and widths. Energy (a,b) and FWHM (c,d) of the plasmonic resonance of individual SMGDs as a function of disk diameter, calculated from quantum (green circles) and classical (orange triangles) models. Results obtained with and without inclusion of *d*-band screening are shown in b and d, and a and c, respectively. The dashed curves in c and d indicate the intrinsic broadening $\hbar\gamma = 71$ meV introduced in the Drude formula (equation (1)) and in the RPA susceptibility (equation (4)).

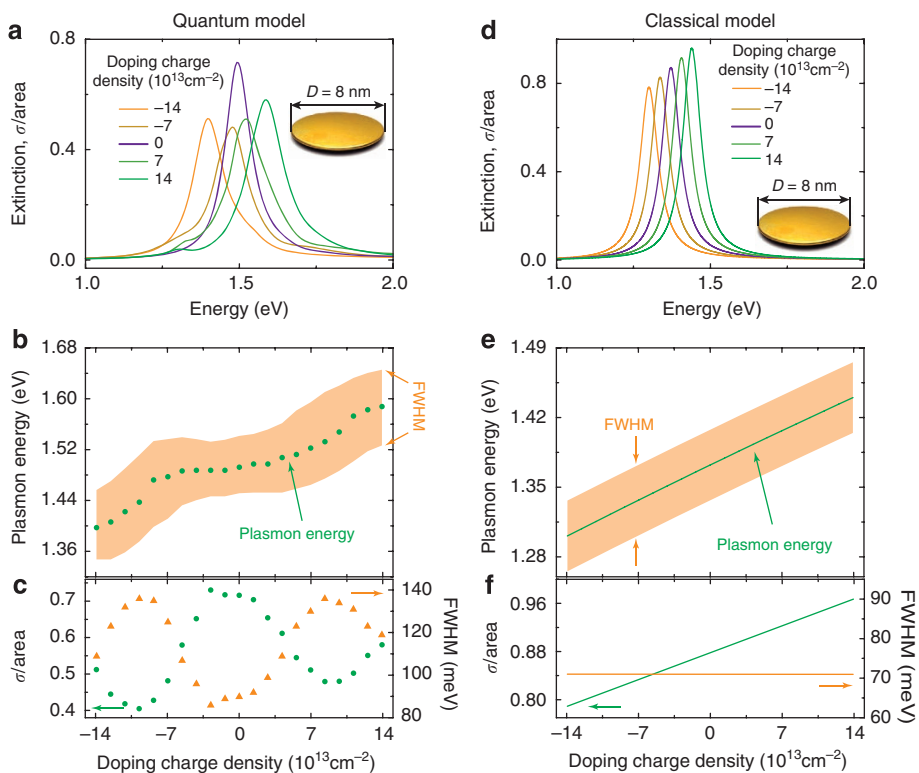


Figure 4 | Quantum versus classical analysis of the electrically tunable optical response. (a,d) Extinction cross-section normalized to the geometrical area for a $D = 8$ nm SMGD calculated with different doping charge densities. (b,e) Plasmon energy as a function of doping charge density. We indicate the FWHM of the plasmon resonances as shadowed regions. (c,f) Optical extinction cross-section at the plasmon peak energy (green curves and symbols, left scale) and FWHM (orange, right scale) as a function of doping density. Quantum mechanical calculations (a-c) are compared with classical results (d-f), including *d*-band screening in all cases.

s-band electron density. The potential of patterned gold monolayers for electro-optical modulation in the NIR is thus excellent.

Discussion

In summary, we have simulated both classically and quantum mechanically the plasmonic response and performance in

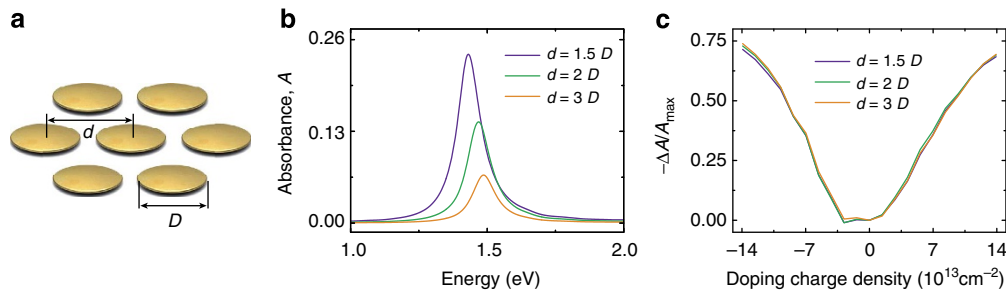


Figure 5 | Electrical modulation of the absorbance of an hexagonal periodic arrangement of SMGDs. (a) Scheme of the system under study. (b) Absorbance spectrum of undoped nanodisks (diameter $D = 8$ nm) for different values of the array spacing d . (c) Modulation of the absorbance relative to the undoped state as a function of doping charge density for different array spacings.

electro-optical modulation of gold nanodisks carved from a single (111) atomic layer. Our RPA calculations incorporate the wave functions of free s -valence electrons evolving in a circular box, as well as an adjusted distribution of dipoles to account for d -band screening. Despite the atomic thickness of the disks, this quantum mechanical description converges smoothly to the results of classical dielectric theory, based on the bulk, frequency-dependent dielectric function of gold. This is a remarkable result, which can be intuitively understood from the fact that the electron current associated with the plasmons flows along the gold layer and, thus, it is rather insensitive to electron confinement within the small film thickness. Nonetheless, non-locality plays a crucial role, leading to strong plasmon blue shifts, as well as splitting due to the complex interaction with the d band. We estimate that non-local effects become dominant when the disk diameter is below ~ 10 nm.

Remarkably, the disks interact strongly with light, giving rise to extinction cross-sections exceeding their geometrical areas in the vis-NIR. We have also shown that the optical response of SMGDs can be efficiently modulated through the addition or removal of realistic concentrations of doping charge carriers using, for example, gating technology. In particular, periodic patterns of monolayer gold appear to be a suitable solution for combining strong plasmonic response and high doping, for example, using an electrical backgate, because the average charge density of the layer is simply determined by capacitor theory for a fixed distance from the gate and, thus, the actual doping charge density in the metal scales with the inverse of the areal filling fraction occupied by the gold. Similar results are expected for films consisting of only a few atomic layers, although the degree of modulation is then reduced because the doping charge has to be shared across the increased thickness. Other plasmonic metals such as silver and copper should find similar degree of tunability (see Supplementary Fig. 5). In particular, the small plasmon width of silver compared with gold makes it an attractive candidate to drive plasmon shifts well beyond the FWHM. In addition, the lower d -band screening in this material should result in higher plasmon energies, reaching the visible in small disks or, equivalently, the NIR for larger disk diameters.

It should be stressed that, while the synthesis of single-layer gold is a mature field²⁸, the fabrication of laterally confined thin gold nanostructures represents a technical challenge, which could benefit from advances in lithography and self-assembly. Alternatively, one could use a continuous gold layer, which also exhibits large electrical tunability of its propagating plasmons (see Supplementary Fig. 6), coupled to external light by decorating it with dielectric colloids to bridge the light-plasmon momentum mismatch (that is, this is essentially what nanostructuring does in the SMGDs that we study above). The resulting planar structures hold great potential for light modulation at vis-NIR frequencies, which could be the basis of a new generation of

electrically tunable optical devices with applications ranging from sensing to nanoscale spectral photometry.

Methods

Quantum mechanical RPA simulations. We consider small disk sizes compared with the light wavelength, so that we work in the electrostatic limit. Within this approximation, assuming an overall monochromatic time dependence $e^{-i\omega t}$ with frequency ω , the induced charge density ρ^{ind} can be expressed in terms of the self-consistent potential ϕ as

$$\rho^{\text{ind}}(\mathbf{r}, \omega) = \int d^3\mathbf{r}' \chi^0(\mathbf{r}, \mathbf{r}', \omega) \phi(\mathbf{r}', \omega) \equiv \chi^0 \cdot \phi, \quad (2)$$

where χ^0 is the non-interacting susceptibility associated with the s -valence electrons of gold, and the last identity defines a matrix notation in which matrix multiplication involves integration over space coordinates. We obtain χ^0 within the RPA⁴¹ in which a one-electron picture is assumed and only individual electron-hole pair excitations are explicitly considered. We further approximate the wave functions of valence electrons by the solutions of a cylindrical box with the same diameter as the nanodisk and a thickness corresponding to the separation between (111) atomic planes in bulk gold (that is, $a_0/\sqrt{3} \approx 0.236$ nm, see Fig. 1a). More precisely,

$$\psi_{lm}(\mathbf{r}) = N_{lm} J_m(Q_{lm} R) e^{im\phi} g_l(z), \quad (3)$$

where N_{lm} is a normalization constant, $Q_{lm} = 2\zeta_{lm}/D$, ζ_{lm} is the l th zero of the Bessel function J_m and $g_l(z) = \sin(\pi\sqrt{3}z/a_0)$ yields the dependence on the coordinate z normal to the disk. For simplicity, we are assuming that the z dependence is separable in the wave function, so that electron diffraction effects at the disk edges are not important. Moreover, we assume that the electrons remain in the ground state of the vertical cavity of thickness $a_0/\sqrt{3}$, which is a reasonable approximation if we consider that the first excited state (that is, $g_2(z) = \sin(2\pi\sqrt{3}z/a_0)$) lies ~ 20 eV above g_1 , well beyond the Fermi and vacuum levels.

With the wave functions of equation (3), we can write the susceptibility as

$$\chi^0(\mathbf{r}, \mathbf{r}', \omega) = \frac{2e^2}{\hbar} \sum_{l,l',m,m'} (f_{l'm'} - f_{lm}) \frac{\psi_{lm}(\mathbf{r}) \psi_{l'm'}^*(\mathbf{r}') \psi_{l'm'}^*(\mathbf{r}) \psi_{lm}(\mathbf{r}')}{\omega - \epsilon_{lm} + \epsilon_{l'm'} + i\gamma/2}, \quad (4)$$

where spin degeneracy is simply included through an overall factor of 2, $\hbar\epsilon_{lm} = \hbar^2 Q_{lm}^2/2m_e$ is the energy of state ψ_{lm} (notice that the energy associated with z motion cancels out in equation (4), so we disregard it), γ is an intrinsic relaxation time, which we take from a Drude fit (equation (1)) to measured optical data²⁹ ($\hbar\gamma = 71$ meV), and $f_{lm} = \{\exp[(\epsilon_{lm} - E_F)/k_B T] + 1\}^{-1}$ is the Fermi-Dirac distribution function, evaluated here at $T = 0$. The method used to fill the energy levels in the disk has been discussed in Supplementary Fig. 3.

The total potential ϕ is the sum of the external potential ϕ^{ext} and the potential produced by the induced charges

$$\phi = \phi^{\text{ext}} + v \cdot \rho^{\text{ind}}, \quad (5)$$

where $v(\mathbf{r}-\mathbf{r}') = 1/|\mathbf{r}-\mathbf{r}'|$ is the Coulomb interaction. From here and equation (2), we solve the induced charge density as

$$\rho^{\text{ind}} = \chi^0 \cdot (1 - v \cdot \chi^0)^{-1} \cdot \phi^{\text{ext}}.$$

As the polarization along the direction normal to the disk is expected to be negligible, we focus on parallel components and write $\phi^{\text{ext}} = -\text{Re}^{i\phi}$ (that is, we focus on solutions with $m = 1$ azimuthal symmetry), where ϕ is the azimuthal angle of (x, y) and $R = \sqrt{x^2 + y^2}$. This allows us to obtain the in-plane polarizability by calculating

$$\alpha(\omega) = \frac{1}{2} \int d^3\mathbf{r} \text{Re}^{-i\phi} \rho^{\text{ind}}(\mathbf{r}, \omega).$$

Finally, the extinction cross-section is obtained from

$$\sigma(\omega) = (4\pi\omega/c)\text{Im}\{\alpha(\omega)\}.$$

Inclusion of d -band screening. Deeper electrons in the d band are relatively localized in the gold atoms and, therefore, we model them by assuming a background of polarizable point particles at the atomic positions in the (111) layer (see lower part of Fig. 1a). The polarizability α_b of these particles is adjusted to fit the experimentally measured bulk dielectric function of gold ϵ_{exp} . That is, if we subtract the Drude s -band contribution from ϵ_{exp} (see equation (1)), we obtain the background permittivity $\epsilon_b = \epsilon_{\text{exp}} + \omega_p^2/(\omega + i\gamma)$, where $\omega_p^2 = 4\pi e^2 n_0/m_e$ is determined by the s -band electron density $n_0 = 4/a_0^3 \approx 5.9 \times 10^{28} \text{ m}^{-3}$. This yields $\hbar\omega_p \approx 9.01 \text{ eV}$, which is slightly different from the best fit of equation (1) to measured data²⁹ (9.06 eV), from which we also find $\epsilon_b = 9.5$. Now, the Clausius–Mossotti relation⁴³ leads to

$$\alpha_b = \frac{3}{4\pi n_0} \frac{\epsilon_b - 1}{\epsilon_b + 2}.$$

Using dyadic notation, the susceptibility tensor of the background dipoles reduces to $\chi_b^0(\mathbf{r}, \mathbf{r}') = \sum_j \bar{\nabla} \cdot \alpha_b \delta(\mathbf{r} - \mathbf{r}_j) \delta(\mathbf{r}' - \mathbf{r}_j) \cdot \bar{\nabla}'$, where j runs over the positions of the metal atoms, whereas $\bar{\nabla}$ ($\bar{\nabla}'$) acts on \mathbf{r} -dependent (\mathbf{r}' -dependent) functions to the left (right) of operator χ_b^0 . As the charge induced through both s and d bands contribute together to the full potential, we can rewrite equation (2) as

$$\rho^{\text{ind}} = (\chi^0 + \chi_b^0) \cdot \phi$$

to take into account the effect of d -band screening. Using this expression together with equation (5), the total induced charge density becomes

$$\rho^{\text{ind}} = (\chi^0 + \chi_b^0) \cdot [1 - v \cdot (\chi^0 + \chi_b^0)]^{-1} \cdot \phi^{\text{ext}},$$

from which we calculate the disk polarizability and the extinction cross-section as explained above.

References

- Novotny, L. & Hecht, B. *Principles of Nano-Optics* (Cambridge Univ. Press, 2006).
- Halas, N. J., Lal, S., Chang, W., Link, S. & Nordlander, P. Plasmons in strongly coupled metallic nanostructures. *Chem. Rev.* **111**, 3913–3961 (2011).
- Álvarez-Puebla, R. A., Liz-Marzán, L. M. & García de Abajo, F. J. Light concentration at the nanometer scale. *J. Phys. Chem. Lett.* **1**, 2428–2434 (2010).
- Atwater, H. A. & Polman, A. Plasmonics for improved photovoltaic devices. *Nat. Mater.* **9**, 205–213 (2010).
- Knight, M. W., Sobhani, H., Nordlander, P. & Halas, N. J. Photodetection with active optical antennas. *Science* **332**, 702–704 (2011).
- O’Neal, D. P., Hirsch, L. R., Halas, N. J., Payne, J. D. & West, J. L. Photo-thermal tumor ablation in mice using near infrared-absorbing nanoparticles. *Cancer Lett.* **209**, 171–176 (2004).
- Grzelczak, M., Pérez-Juste, J., Mulvaney, P. & Liz-Marzán, L. M. Shape control in gold nanoparticle synthesis. *Chem. Soc. Rev.* **37**, 1783–1791 (2008).
- Stokes, N., McDonagh, A. M. & Cortie, M. B. Preparation of nanoscale gold structures by nanolithography. *Gold Bull.* **40/4**, 310–320 (2007).
- Mulvaney, P., Pérez-Juste, J., Giersig, M., Liz-Marzán, L. M. & Pecharrómán, C. Drastic surface plasmon mode shifts in gold nanorods due to electron charging. *Plasmonics* **1**, 61–66 (2006).
- Chu, K. C., Chao, C. Y., Chen, Y. F., Wu, Y. C. & Chen, C. C. Electrically controlled surface plasmon resonance frequency of gold nanorods. *Appl. Phys. Lett.* **89**, 103107 (2006).
- Boardman, A. D. *et al.* Active and tunable metamaterials. *Laser Photon. Rev.* **10**, 00012 (2010).
- Liu, A. Q., Zhu, W. M., Tsai, D. P. & Zheludev, N. I. Micromachined tunable metamaterials: a review. *J. Opt.* **14**, 114009 (2012).
- Armelles, G., Cebollada, A., García-Martín, A. & González, M. U. Magnetoplasmonics: combining magnetic and plasmonic functionalities. *Adv. Opt. Mater.* **1**, 10–35 (2013).
- Feigenbaum, E., Diest, K. & Atwater, H. A. Unity-order index change in transparent conducting oxides at visible frequencies. *Nano Lett.* **10**, 2111–2116 (2010).
- Abb, M., Albella, P., Aizpurua, J. & Muskens, O. L. All-optical control of a single plasmonic nanoantenna-ITO hybrid. *Nano Lett.* **11**, 2457–2463 (2011).
- Comin, A. & Manna, L. New materials for tunable plasmonic colloidal nanocrystals. *Chem. Soc. Rev.* doi:10.1039/C3CS60265F (2014).
- Castro Neto, A. H., Guinea, F., Peres, N. M. R., Novoselov, K. S. & Geim, A. K. The electronic properties of graphene. *Rev. Mod. Phys.* **81**, 109–162 (2009).
- Jablan, M., Buljan, H. & Soljačić, M. Plasmonics in graphene at infrared frequencies. *Phys. Rev. B* **80**, 245435 (2009).
- Koppens, F. H. L., Chang, D. E. & García de Abajo, F. J. Graphene plasmonics: a platform for strong light-matter interactions. *Nano Lett.* **11**, 3370–3377 (2011).
- Grigorenko, A. N., Polini, M. & Novoselov, K. S. Graphene plasmonics. *Nat. Photon.* **6**, 749–758 (2012).
- Chen, J. *et al.* Optical nano-imaging of gate-tunable graphene plasmons. *Nature* **487**, 77–81 (2012).
- Fei, Z. *et al.* Gate-tuning of graphene plasmons revealed by infrared nano-imaging. *Nature* **487**, 82–85 (2012).
- Fang, Z. *et al.* Gated tunability and hybridization of localized plasmons in nanostructured graphene. *ACS Nano* **7**, 2388–2395 (2013).
- Ju, L. *et al.* Graphene plasmonics for tunable terahertz metamaterials. *Nat. Nanotechnol.* **6**, 630–634 (2011).
- Brar, V. W., Jang, M. S., Sherrott, M., Lopez, J. J. & Atwater, H. A. Highly confined tunable mid-infrared plasmonics in graphene nanoresonators. *Nano Lett.* **13**, 2541–2547 (2013).
- Manjavacas, A., Thongrattanasiri, S. & García de Abajo, F. J. Plasmons driven by single electrons in graphene nanoislands. *Nanophotonics* **2**, 139–151 (2013).
- Manjavacas, A. *et al.* Tunable molecular plasmons in polycyclic aromatic hydrocarbons. *ACS Nano* **7**, 3635–3643 (2013).
- Green, A. & Bauer, E. Gold monolayers on silicon single crystal surfaces. *Surf. Sci.* **103**, L127–L133 (1981).
- Johnson, P. B. & Christy, R. W. Optical constants of the noble metals. *Phys. Rev. B* **6**, 4370–4379 (1972).
- García de Abajo, F. J. & Howie, A. Retarded field calculation of electron energy loss in inhomogeneous dielectrics. *Phys. Rev. B* **65**, 115418 (2002).
- Rakić, A. D., Djurišić, A. B., Elazar, J. M. & Majewski, M. L. Optical properties of metallic films for vertical-cavity optoelectronic devices. *Appl. Opt.* **37**, 5271–5283 (1998).
- Thongrattanasiri, S., Silveiro, I. & García de Abajo, F. J. Plasmons in electrostatically doped graphene. *Appl. Phys. Lett.* **100**, 201105 (2012).
- Lang, N. D. & Kohn, W. Theory of metal surfaces: charge density and surface energy. *Phys. Rev. B* **1**, 4555–4568 (1970).
- Zuloaga, J., Prodan, E. & Nordlander, P. Quantum description of the plasmon resonances of a nanoparticle dimer. *Nano Lett.* **9**, 887–891 (2009).
- Savage, K. J. *et al.* Revealing the quantum regime in tunnelling plasmonics. *Nature* **491**, 574–577 (2012).
- Kreibig, U. & Vollmer, M. *Optical Properties of Metal Clusters* (Springer-Verlag, 1995).
- Liebsch, A. Surface-plasmon dispersion and size dependence of Mie resonance: silver versus simple metals. *Phys. Rev. B* **48**, 11317–11328 (1993).
- Onida, G., Reining, L. & Rubio, A. Electronic excitations: density-functional versus many-body Green’s-function approaches. *Rev. Mod. Phys.* **74**, 601–659 (2002).
- Sakko, A., Rossi, T. P., Enkovaara, J. & Nieminen, R. M. Atomistic approach for simulating plasmons in nanostructures. *Appl. Phys. A* doi:10.1007/s00339-013-8034-3 (2013).
- Lisnetskaya, P. G. & Mitrić, R. *Ab initio* simulations of light propagation in silver cluster nanostructures. *Phys. Rev. B* **89**, 035433 (2014).
- Pines, D. & Nozières, P. *The Theory of Quantum Liquids* (W. A. Benjamin Inc., 1966).
- Thongrattanasiri, S., Koppens, F. H. L. & García de Abajo, F. J. Complete optical absorption in periodically patterned graphene. *Phys. Rev. Lett.* **108**, 047401 (2012).
- Ashcroft, N. W. & Mermin, N. D. *Solid State Physics* (Harcourt College Publishers, 1976).

Acknowledgements

This work has been supported in part by the European Commission (Graphene Flagship CNECT-ICT-604391 and FP7-ICT-2013-613024-GRASP). A.M. acknowledges financial support from the Spanish MEC through the FPU programme and from the Evans Attwell-Welch Postdoctoral Fellowship for Nanoscale Research, administered by the Richard E. Smalley Institute for Nanoscale Science and Technology.

Author contributions

F.J.G.d.A. proposed the study. A.M. and F.J.G.d.A. worked out the theory, discussed the results and wrote the paper. A.M. performed the numerical calculations.

Additional information

Supplementary Information accompanies this paper at <http://www.nature.com/naturecommunications>

Competing financial interests: The authors declare no competing financial interests.

Reprints and permission information is available online at <http://npg.nature.com/reprintsandpermissions/>

How to cite this article: Manjavacas, A. & García de Abajo, F. J. Tunable plasmons in atomically thin gold nanodisks. *Nat. Commun.* 5:3548 doi: 10.1038/ncomms4548 (2014).